



Article

Analysis of Pore Characterization and Energy Evolution of Granite by Microwave Radiation

Keping Zhou, Yifan Zhang, Chun Yang , Niange Yang and Zheng Pan *

School of Resources and Safety Engineering, Central South University, Changsha 410083, China

* Correspondence: panzheng@csu.edu.cn

Abstract: To study the dynamic response of granite to different levels of microwave power, an intelligent microwave rock-breaking instrument is used to irradiate different power from three directions. The servo universal testing machine is used to carry out a uniaxial compression test on the granite after microwave damage to analyze the strength damage characteristics and the degree of pore damage. Pore fractal characteristics are analyzed based on nuclear magnetic resonance to establish the microwave damage degradation model. In parallel, the energy evolution process of granite under the influence of various power levels is analyzed using the theory of energy dissipation. Simultaneously, based on the energy dissipation theory, we analyze the energy evolution process of granite under the action of different powers. The results show that with higher microwave power, the peak strength and modulus of elasticity show a linear decreasing law. The degree of fragmentation is more obvious, showing the damage characteristics with two big ends and little in the middle. The higher the power, the greater the porosity and the more sensitive the micropore becomes to microwaves. Additionally, the damage degradation model established to evaluate the microwave damage of the rock showed that it was feasible. The higher the power, the lower the total energy, elastic energy, and dissipation energy, and the granite is gradually transformed from elastic deformation to plastic deformation. The elastic energy ratio decreases, the dissipation energy ratio increases, and the degree of damage becomes more and more serious. This study provides theoretical support for exploring the mechanical behavior and mechanism of microwave-assisted rock breaking and is of great practical significance.



Citation: Zhou, K.; Zhang, Y.; Yang, C.; Yang, N.; Pan, Z. Analysis of Pore Characterization and Energy Evolution of Granite by Microwave Radiation. *Fractal Fract.* **2024**, *8*, 161. <https://doi.org/10.3390/fractalfract8030161>

Academic Editors: Zine El Abiddine Fellah, Mei Yin, Mengxi Zhang and Yi Rui

Received: 7 January 2024
Revised: 29 February 2024
Accepted: 2 March 2024
Published: 12 March 2024



Copyright: © 2024 by the authors. Licensee MDPI, Basel, Switzerland. This article is an open access article distributed under the terms and conditions of the Creative Commons Attribution (CC BY) license (<https://creativecommons.org/licenses/by/4.0/>).

Keywords: NMR; microwave; damage; hard rock; energy

1. Introduction

The present large demand for mineral resources and mining uses drilling, blasting, and mechanical rock-breaking methods [1–3], which utilize mechanical impact, cutting, or impact–cutting composite effects. These methods cause hard rock tensile shear composite damage and mechanical rock-breaking tool wear, which are the main problems faced [4,5]. Microwaves are a fast and effective means of assisting in rock breaking so that dielectric molecular polarization phenomenon occurs within the rock and, at the same time, causes internal chemical bond breakage and rearrangement combinations, thus reducing the rock bearing capacity. In addition, rock contains a variety of mineral components, which effectively absorb temperature, making the rock surface temperature increase, expand, and rupture. Microwave irradiation can significantly reduce the strength of many common rocks and enhance the effect of mechanical rock breaking. However, the actual engineering situation is complex and influenced by many factors. The technology is still in the experimental stage; it has not formed a mature theoretical system to guide the engineering application.

In recent years, many scholars have carried out research on rock properties after microwave irradiation, mainly focusing on indoor experiments, numerical simulation, and theoretical research. Ma, Z et al. [6] studied the temperature, ultrasonic velocity, and

intensity changes after microwave irradiation of amphibolite and found that the temperature rises greatly after microwave irradiation, the speed of the wave decreases, and the microwave treatment can greatly weaken the strength of the specimen and improve the efficiency of the impact of a hammer in rock breaking. Feng, X et al. [7] studied the crack extension characteristics of microwave-irradiated hard rocks with different rotational speeds under true triaxial stress and showed that the higher the rotational speed of microwave irradiation, the higher the degree of crack extension in hard rocks, the development of a more dense, more complex crack network, and the form of damage mainly in the form of tensile damage. Zou, C et al. [8] studied the static and dynamic mechanical characteristics of microwave irradiation of hard rocks and found that short-time microwave radiation causes severe damage to rocks. Under static tests, uniaxial compressive strength, Brazilian tensile strength, indentation hardness, and impact strength all decreased to different degrees. Furthermore, it was found that tensile strength was the most sensitive to microwaves, while crack density was the least sensitive to microwaves. Most scholars include additives in order to improve the effect of microwave radiation [9,10]. Gao, F et al. [11] studied the degree of microwave absorption in barium-titanate-suspension-immersed rocks and water-saturated rocks and found that the wave-treated P-wave velocity, porosity, and strength appeared to cause more serious damage, and at the same time, the barium titanate suspension rocks absorbed microwaves better than water-saturated rocks. To carry out multi-faceted research, studies have compared traditional heating and microwave heating [12], unilateral and bilateral heating [13], cyclic microwave irradiation [14], and so on. Microwave damage to rock is complex and difficult to analyze with general mechanical properties. Since the deformation damage of rock is mainly due to energy dissipation, it is a very effective method to reveal microwave radiation damage by using energy dissipation theory. Yang, J et al. [15], Tang, M et al. [16], and Hassani, F et al. [17] analyzed the loaded energy evolution process of rocks after microwave damage based on the dissipated energy theory, and the results showed that the weakening of rocks by microwave irradiation not only reduces the degree of energy storage in rocks and increases the proportion of its dissipated energy during the damage process, but also reduces the rate of elastic energy release after the peak. Most of the studies on microwave numerical simulation are based on COMSOL finite element software. Pressacco, M et al. [18,19] simulated the uniaxial compression test and tensile test of two-dimensional and three-dimensional rocks damaged by microwaves based on the damage-viscoelasticity model. Zhao, X et al. [20] used COMSOL multiphysics to perform numerical simulations to obtain temperature and stress distributions inside the rock, and Rui, F et al. [21] developed a fine-grained multi-physics system by combining the concepts of grain-based modeling (GBM), electromagnetic thermal solution of COMSOL, and the thermo-mechanical fracture simulation of four-dimensional lattice spring model (4D-LSM). Some scholars have explored the microwave-rock interaction mechanism from the mineral point of view in combination with macro and fine-scale tests. Lu, G et al. [22], Tian, J et al. [23], Hartlieb, P et al. [24], and Zhao, Q et al. [10] investigated the effect of microwaves on the heating of minerals inside the rock. Lu, G et al. [25] suggest that the anisotropy of some minerals absorbs heat and provides heat to other minerals, which exceeds the carrying capacity of the minerals, leading to rock damage rupture. Currently, there are fewer studies on pore changes in microwave-damaged rocks [26,27]. Yao, J et al. [28] used nuclear magnetic resonance (NMR) to study the changes in porosity after microwave irradiation, resulting in the formation of transgranular fractures and an increase in the number of intergranular fractures. Li, X et al. [29] used nuclear magnetic resonance (NMR) to study the dynamic tensile behavior of granite under different microwave powers and found that the microwave heating promoted the simplification of the pore structure, manifested as a change in the pore size distribution from bimodal to trimodal, and decreased the fractal dimension of the macropores. Ding, R et al. [30] investigated the pore changes in gabbro under different irradiation times of microwaves and found that with the increase in microwave irradiation time, the porosity and permeability of gabbro increased,

and the surface cracks of gabbro were mainly intergranular cracks and then transcrySTALLINE cracks within 10 min of microwave irradiation.

Porosity is an important parameter reflecting the mechanical characteristics of rock. The action of microwaves increases both the porosity and the number of microcracks within the rock, leading to rock damage. Rock loading characterizes the release of internally stored elastic energy to the exterior, and by examining energy evolution, one can reflect on changes in the mechanical properties of damaged rock. If microwave irradiation power is too high, it results in effective rock breaking, but also in significant resource waste. Therefore, studying the changes in granite porosity and energy evolution under different microwave power levels is crucial for optimally controlling microwave power in real engineering projects, thereby improving economic efficiency. Consequently, addressing the issue of wear on TBM (tunnel boring machine) cutter saws by researching microwave radiation damage in hard rock is an urgent topic and of great significance to real-world engineering. Based on previous research, this study investigates the mechanical properties of granite, along with pore changes and energy dissipation under various microwave power levels, in different directions. It aims to explore the effect of damage weakening in granite under different microwave powers, identify optimal and reasonable microwave irradiation parameters for practical production, and contribute to the theoretical development and engineering application of microwave-assisted rock crushing technology.

2. Experimental Equipment

The experiment utilized granite as the subject of research. The granite was placed in a drying oven for 48 h, after which they were irradiated in different orientations (1 kW, 2 kW, 3 kW) for 240 s using the WLK-A9 intelligent microwave rock-breaking instrument. The porosity changes resulting from microwave damage were measured with an AiniMR-150 NMR instrument. Uniaxial compression tests were carried out using the SHT4206 microcomputer-controlled electro-hydraulic servo universal testing machine. The testing method was displacement-controlled, with a rate of 0.2 mm/min. The flow is shown in Figure 1.

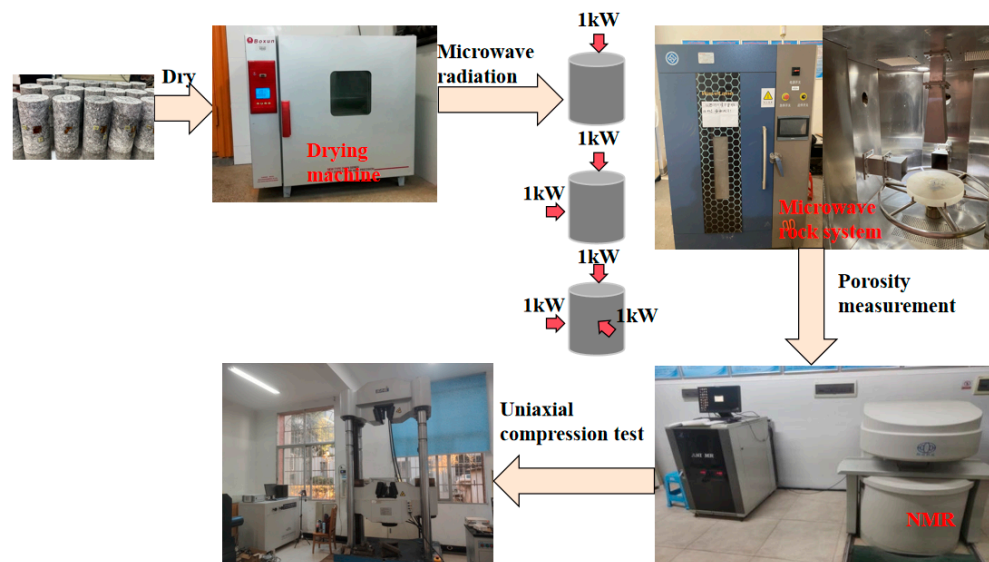


Figure 1. Schematic diagram of test system flow.

3. Analysis of Results

The stress–strain curve of granite under loading encompasses five stages, as shown in Figure 2.

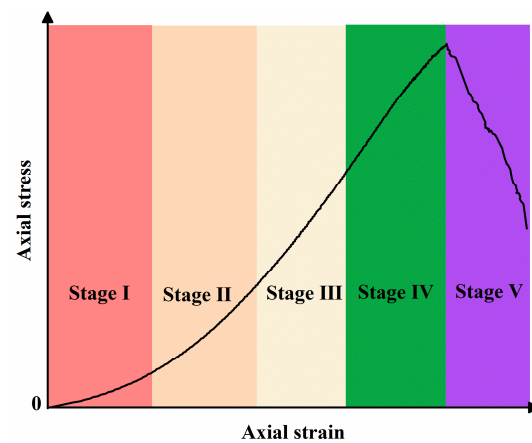


Figure 2. Schematic stress–strain curve.

Stage I (compaction stage): This stage is the initial loading stage of granite. With the increase in axial stress, the specimen internal microcracks, and pore compaction, the curve shows a non-linear growth.

Stage II (elastic deformation stage): As the axial force continues to increase, the curve maintains an approximate straight-line rise, and the deformation is elastic deformation which is reversible upon load removal. Notably, higher microwave power shortens the duration of this stage, hastening the transition to the crack expansion phase. This is attributed to microwaves fostering the nucleation of microcracks within the granite, thereby increasing the likelihood of their propagation.

Stage III (stable crack expansion stage): With further increases in axial force, the curve shows a non-linear growth trend, and the microcracks inside the granite begin to expand, with the density gradually increasing and expanding in the direction of the maximum principal stress.

Stage IV (crack instability and expansion stage): This stage is marked by the accelerated aggregation of cracks, which coalesce into a nucleus as the axial force continues to rise. The expansion rate of microcracks surges, culminating in peak strength and subsequent specimen failure. Higher microwave power is observed to exacerbate this process, primarily due to the severe internal damage it inflicts on the granite, resulting in an abundance of microcracks and microporosity that facilitate swift crack expansion and rapid disintegration.

Stage V (after the damage peak stage): Following the attainment of peak compressive strength, the specimen’s load-bearing capacity diminishes sharply, as reflected by a precipitous decline in the stress–strain curve. The granite exhibits pronounced brittle failure, although the residual strength is sustained to some degree by shear strength and friction along the fracture surfaces.

Figure 3 shows the stress–strain curves for different groups irradiated by microwave powers of 1 kW, 2 kW and 3 kW. Additionally, a control group was established, which did not undergo microwave irradiation. Upon reaching peak strength, the curves immediately drop abruptly, which is called “stress softening”. This phase is characterized by its brief duration and is marked by the abrupt failure of the granite, often accompanied by a distinctive ‘click’ sound. The experimental results indicate that as the microwave power increases, the mode of damage in granite shifts, with higher leading to pronounced brittle damage.

Figure 4 shows the changes in peak strength and elastic modulus of granite under different powers. It can be seen from the figure that with the increase in microwave power, the peak strength and modulus show an almost straight-line decreasing pattern. When the microwave power increases from 0 kW to 3 kW, the peak strength decreases from 227.1 MPa to 174.6 MPa, a decrease of 30.1%, and the elastic modulus decreases from 49 GPa to 40.27 GPa, a decrease of 21.7%. Therefore, microwaves have an obvious deterioration effect on the strength of rocks, and the higher the power, the higher the degree of damage to granite. It can be seen that the microwave-assisted rock-breaking effect is very

obvious. This is mainly because the higher the microwave power, the more microcracks in the internal structure and the lower the load-carrying capacity, which reduces the peak strength and elasticity modulus and changes from ductile to brittle damage.

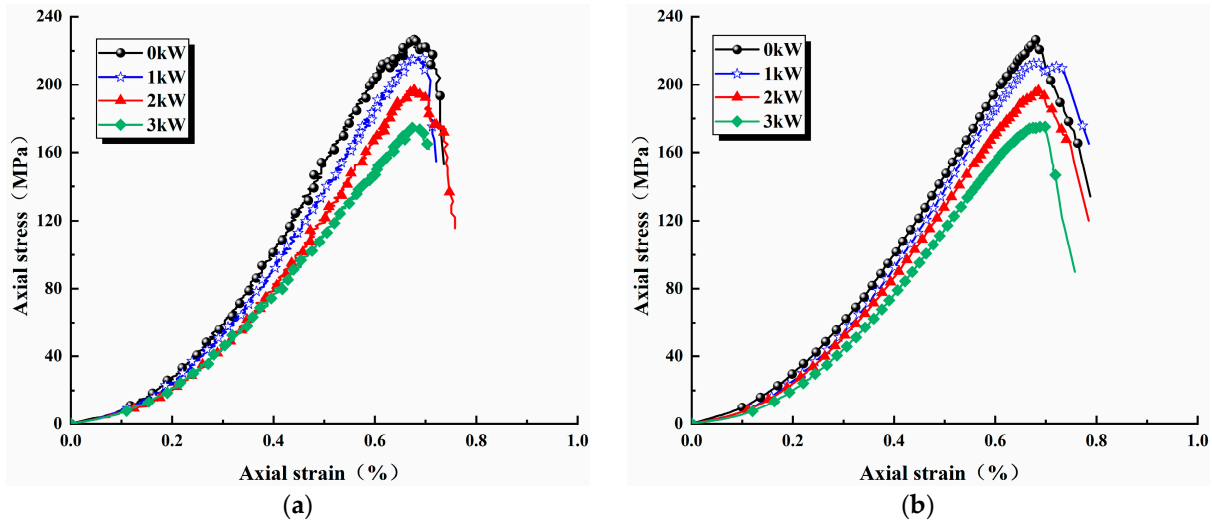


Figure 3. Stress–strain curve. (a) Group A; (b) group B.

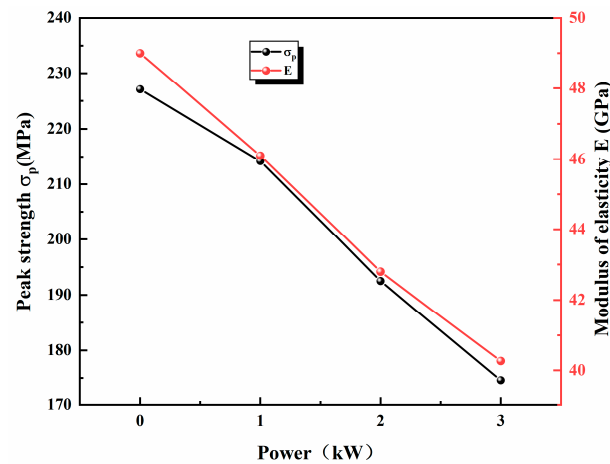


Figure 4. Peak strength and modulus of elasticity versus microwave power.

Figure 5 shows the uniaxial compression damage characteristics of granite under different microwave powers. It can be seen from the figure that in the absence of microwave damage, the granite has undergone obvious compression and shear damage, a shear fracture zone was formed along the granite surface, and some fragments fell off. With the increase in microwave power, the degree of granite fragmentation increased significantly. When the power is 1 kW, there are some large pieces falling from the granite surface; when it is 2 kW, there is a large amount of granite fragments falling, with serious spalling in the middle; when it is 3 kW, the granite has very obvious small fragments peeling off, and the degree of fragmentation is partially deepened. The specific manifestation is that a large number of middle granite fragments fell to form large granite fragments at both ends and small ones in the middle, and the middle granite fragments deepened. This feature is increasingly significant with the higher microwave power.

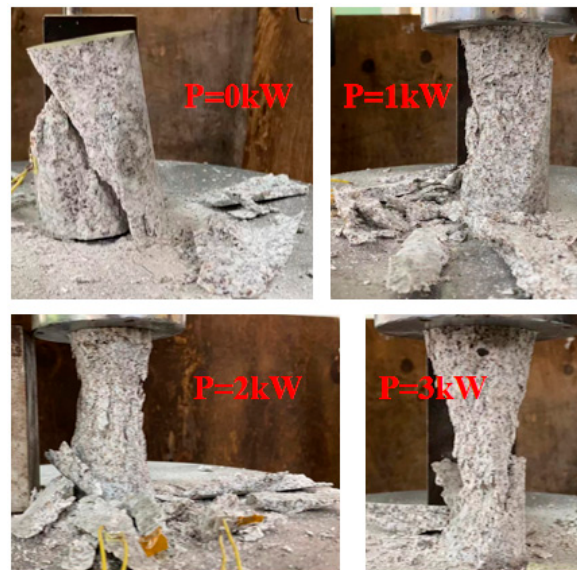


Figure 5. Failure modes of granite under uniaxial compression under different microwave powers.

4. Based on NMR Porosity Analysis

4.1. Effect of Microwaves on Granite Porosity

By detecting different NMR signals, changes in rock pore structure can be directly reflected. T_2 is a time constant that describes the decay of the transverse component of the magnetization. According to the NMR theory, the transverse relaxation rate of NMR can be expressed by the following equation.

$$\frac{1}{T_2} = \frac{1}{T_2^1} + \frac{\rho_2 s}{V} + \frac{D(\gamma G T_E)^2}{12} \quad (1)$$

where T_2^1 is the relaxation time of fluid; ρ_2 is the transverse surface relaxation strength; s is the pore surface area; V is the pore volume; $\frac{\rho_2 s}{V}$ is the transverse surface relaxation rate; D is the diffusion coefficient; γ is the gyromagnetic ratio; G is the magnetic field gradient; T_E is the echo time; $\frac{D(\gamma G T_E)^2}{12}$ is the diffusion relaxation rate. There is only one fluid (water) in the pores and the volume relaxation is much slower than the area relaxation, so $1/T_2^1$ is neglected. The diffusive relaxation rate can also be neglected when the magnetic field is uniform and the T_E time employed is short. Therefore, Formula (1) can be simplified as

$$\frac{1}{T_2} = \frac{\rho_2 s}{V} = \frac{\rho_2 F_2}{r_c} \quad (2)$$

where r_c is the rock pore size and F_2 is the core pore shape factor, which is usually constant and related to the pore shape.

Let $\rho_2 F_2 = C$. In this paper, $C = 10$, then Formula (2) becomes Formula (3) [23].

$$r_c = C T_2 \quad (3)$$

From Formula (3), the T_2 distribution reflects the information on pore size: the smaller the T_2 value, the smaller the pore size; the larger the T_2 value, the larger the pore size.

The T_2 spectral peak curves of granite rocks are divided into different pore types according to the different spectral peaks corresponding to different T_2 values. Based on the experimental capillary pressure measurements of porosity radius grading method, and combined with the relevant literature, the author classified the pore sizes of the red sandstone into three intervals, i.e., small pores ($r \leq 1 \mu\text{m}$), medium pores ($1 \mu\text{m} \leq r \leq 100 \mu\text{m}$), and large pores ($r \geq 100 \mu\text{m}$) [31–33]. Combined with Equation (3), it can be seen that the transverse relaxation time T_2 spectral distribution is from 0 to 10 ms for small holes, from

10 to 100 ms for medium holes, and above 100 ms for large holes. As shown in Figure 6, the T_2 spectrum shows a bimodal pattern, with the first spectral peak for small-size pores (micropores), the second spectral peak for medium-size pores (mesopores), and the second spectral peak followed by large-size pores (macropores or microfractures). According to the above grading criteria, the statistical distribution of different pores in granite is shown in Table 1.

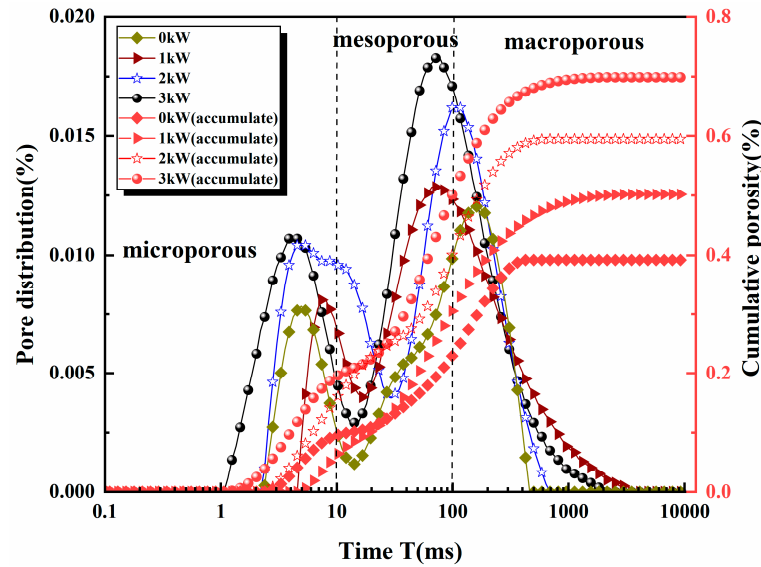


Figure 6. Nuclear magnetic resonance T_2 spectra.

Table 1. Porosity components.

Power (kW)	0	1	2	3
Total porosity (%)	0.392	0.502	0.594	0.699
Microporous (%)	0.094	0.065	0.161	0.193
Mesoporous (%)	0.229	0.305	0.401	0.501
Macroporous (%)	0.069	0.132	0.032	0.002

The cumulative porosity changes under different powers are shown in Figure 6. In the stage of relaxation time less than 10 ms, the cumulative porosity rises slowly, which is mainly microporous development; in the stage of relaxation time from 10 ms to 100 ms, the cumulative porosity rises rapidly, which is mainly medium porosity development; in the stage of relaxation time from 100 ms to 1000 ms, the cumulative porosity rises slowly until it remains constant at a constant value, which is mainly macroporous development. Moreover, the larger the microwave damage, the faster the cumulative porosity rises and the larger the cumulative porosity.

Figure 7 represents the changes in granite porosity under different microwave powers. As can be seen from the figure, as the power increases from 0 kW to 3 kW, the total porosity increases almost linearly, from 0.392% to 0.699%, an increase of 78.3%. The microporosity performance and the total porosity increase almost linearly from 0.229% to 0.501%, an increase of 118.8%. With the power increases, the overall performance of mesoporosity shows an increasing trend from 0.094% to 0.193%, an increase of 105.3%. Macroporosity does not show the corresponding law, indicating that the microwave damage to macroporosity has less impact on microporosity and mesoporosity. The overall porosity is greatly affected by microwaves, so the porosity index can reflect the damage characteristics of the microwave to granite [34,35].

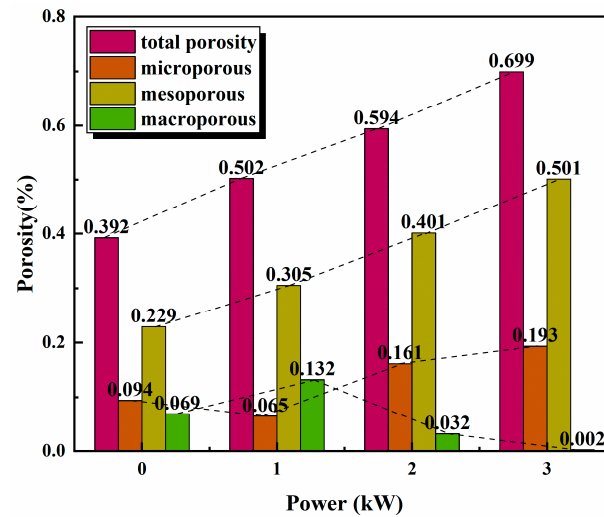


Figure 7. Relationship between porosity and microwave powers.

In order to further reflect the degree of microwave damage to granite, Equation (4) is used to define the damage factor D_N .

$$D_N = 1 - \frac{P_N}{P_0} \quad (4)$$

where P_N is the porosity at different powers and P_0 is the porosity without microwave damage.

Figure 8 indicates the relationship between the microwave damage factor and the power. It can be clearly seen from the figure that as the increase in power, the damage factor rises almost in a straight line, and the degree of damage gradually increases. Under the action of 3 kW, the degree of damage is close to 80%. It can be seen that the degree of microwave damage to granite cannot be ignored.

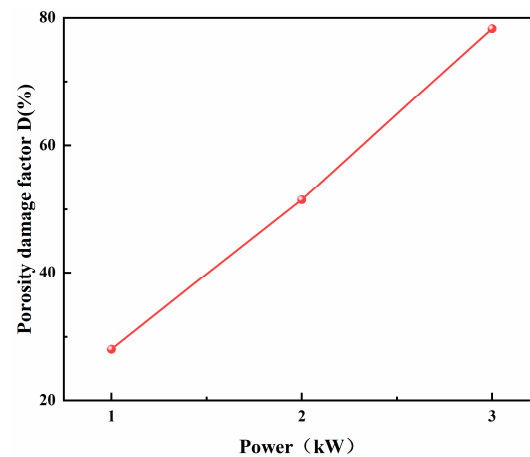


Figure 8. Porosity damage factor.

Figure 9 represents the percentage of microporosity, mesoporosity and macroporosity under different microwave powers. It can be seen that the percentage of microporosity is around 50%, and the percentage of microporosity at 3 kW is only 45.6%, which is reduced compared with other powers, so it can be seen that the percentage of microporosity of the rock is reduced at high power and converted to mesoporosity and macroporosity. The percentage of mesoporosity is around 17%, the percentage of macroporosity is around 32%, and the granite is mainly dominated by microporosity.

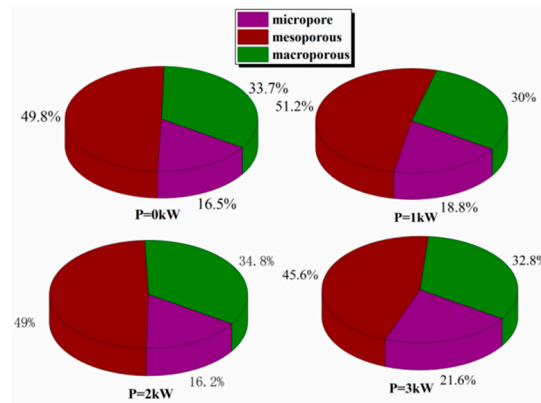


Figure 9. Percentage of different pore sizes.

The primary mechanism of interaction between microwaves and rocks is that characteristic minerals in rocks can absorb microwave energy and then convert it into thermal energy. This transformation increases the temperature of the rock, causing free expansion and thermal stresses at mineral grain boundaries due to compression, ultimately resulting in a reduction in rock strength [36–38]. Granite mainly contains quartz and feldspar, and relevant studies have shown that microwave irradiation of granite, the main internal intracrystalline cracks, cracks along the grain, and cracks through the grain occur [39]. Moreover, the internal damage characteristics of granite are closely related to quartz and plagioclase feldspar, and quartz has good thermal conductivity and coefficient of thermal expansion, which will make the temperature of granite continue to rise, and rupture seriously [40,41]. From the microstructure analysis, we can see that microwaves convert the C-O single bond to a C=O double bond, resulting in the reorganization of the molecular bond, which, in turn, produces damage to the crystal, and at the same time, microwaves have the greatest impact on the molecular SiO₂ and Al₂O₃, which correspond to quartz and feldspar, respectively. Furthermore, pertinent research has demonstrated [22] that metal ions react more strongly to microwaves, that the crystal structures of feldspar and pyroxene exhibit a much smaller bonding capacity when a large number of metal ions are present than when other molecular bonding occurs, and that metal ions can effectively increase the molecular polar ability.

4.2. Porosity Fractal Characterization

Since the porosity distribution is irregular and complex, using simple geometric formulas to describe it is not at all insightful. However, it can be investigated using fractal theory, i.e., it can be characterized using fixed non-integer dimensions between Euclidean dimensions [42]. The fractal dimension is a quantitative parameter that describes the degree of irregularity of a fractal object. The degree of irregularity of fractal objects can indirectly reflect the complexity and irregularity of pore structure. According to the fractal theory [43], the number of pores n with diameters greater than r satisfies the following functional relationship.

$$n(> r) = \int_r^{r_{max}} I(r) dr = ar^{-D} \quad (5)$$

The volume of a pore with a diameter less than r is denoted as:

$$V(< r) = \int_{r_{min}}^r I(r) ar^3 dr \quad (6)$$

where r_{min} and r_{max} are the minimum and maximum porosity, respectively; $I(r)$ is the pore size distribution density; a is a constant; and D is the pore fractal dimension.

Combining Equations (5) and (6) yields.

$$V(< r) = \beta \left(r^{3-D} - r_{min}^{3-D} \right) \tag{7}$$

where β is a constant.

The cumulative pore volume fraction for pore sizes less than r is expressed as:

$$S_V = \frac{V(< r)}{V_S} = \frac{r^{3-D} - r_{min}^{3-D}}{r_{max}^{3-D} - r_{min}^{3-D}} \tag{8}$$

V_S is the total porosity.

Since $r_{min} \ll r_{max}$, Equation (8) can be simplified to:

$$S_V = \frac{r^{3-D}}{r_{max}^{3-D}} \tag{9}$$

According to Equation (3) T_2 and r are proportional, so Equation (9) can be written as:

$$S_V = \left(\frac{T_2}{T_{2,max}} \right)^{3-D} \tag{10}$$

where $T_{2,max}$ is the maximum relaxation time.

Taking the logarithm on both sides of Equation (10) yields

$$\lg S_V = (3 - D)\lg T_2 + (D - 3)\lg T_{2,max} \tag{11}$$

Accordingly, the porosity fractal dimension can be obtained by taking the logarithm of the NMR technique porosity distribution curve and fitting a linear regression to Equation (11) with a slope of the regression curve of $(3 - D)$, see Figure 10, and the results are shown in Table 2.

Table 2. NMR fractal dimensions.

Fractal Dimensions	Power (kW)			
	0	1	2	3
D_{min}	0.911	0.282	0.103	0.02
D_{max}	2.812	2.824	2.734	2.779

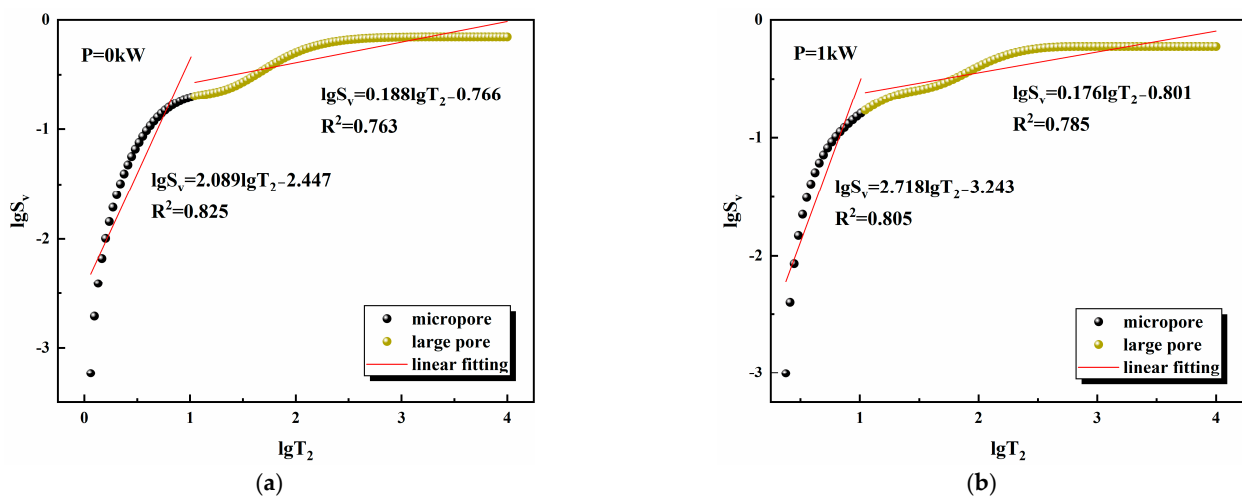


Figure 10. Cont.

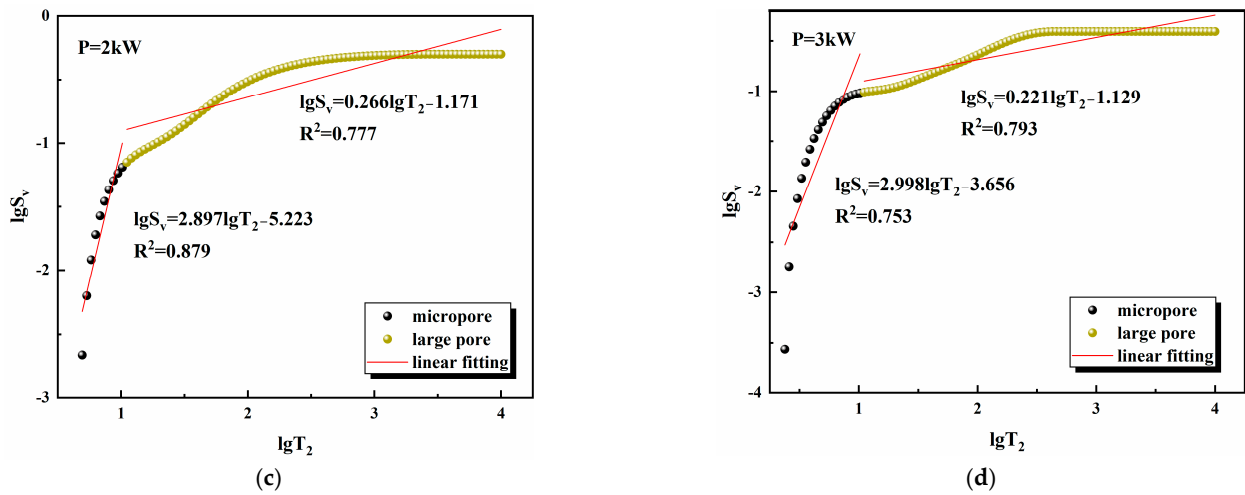


Figure 10. NMR fractal characterization. (a) P = 0 kW; (b) P = 1 kW; (c) P = 2 kW; (d) P = 3 kW.

Figure 11 represents the fractal dimension versus power. From the figure, it can be seen that the fractal dimension D_{min} shows an approximate exponential function decreasing law with the increase in power, while there is no correlation shown between D_{max} and power, so the microwave has more influence on the microporosity of granite than the macroporosity, and it is necessary to take the condition of microporosity into account in the actual microwave-assisted rock-breaking project.

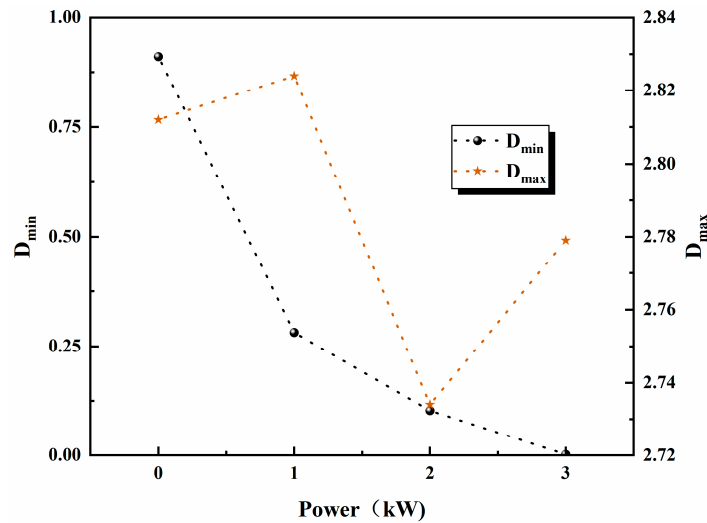


Figure 11. Relationship between fractal dimension and microwave power.

4.3. Microwave Deterioration Damage Model

The most obvious effect of microwaves on granite is the change in porosity, and in Equation (12), the microwave damage factor is used to describe the pore destruction process.

$$W_t = \frac{1 - P_N}{1 - P_0} \tag{12}$$

where W_t is the damage factor. Only the damage factor can not describe the granite microwave damage porosity change characteristics; here, the introduction of coefficient γ , so the damage factor W can be expressed as:

$$W = \gamma W_t \tag{13}$$

$$\gamma = 1 - \frac{D_{0,min}}{D_{N,min}} \tag{14}$$

To investigate the relationship between the peak intensity correlation coefficient and the damage factor, the model studied by Gao et al. [44] is fitted.

$$\frac{\sigma_N}{\sigma_0} = \eta \exp(-\rho\Delta W) \tag{15}$$

where η and ρ are the correlation coefficients; ΔW is the change in damage factor, $\Delta W = W_N - W_0$.

Through Figure 12, it can be seen that the UCS correlation coefficient shows an exponential function growth trend with Δw , and the fitting $R^2 = 0.999$, which is good. It can be seen that the damage growth model can further reflect the degree of microwave damage to granite.

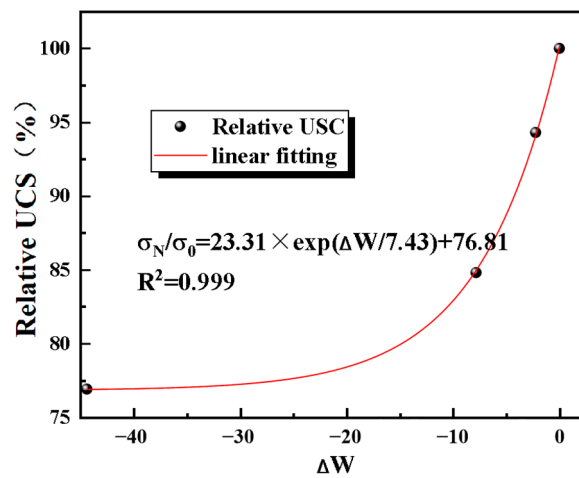


Figure 12. Relationship between UCS and ΔW .

5. Energy Evolution Analysis

It is assumed that granite is in a closed system with no energy exchange conditions with the external environment. According to the first law of thermodynamics, it can be assumed that all the external work is converted into energy storage and dissipation during the deformation of the rock, so the whole energy consists of two parts: elastic energy and dissipation energy [45,46], and the total energy U , the elastic energy U_e , and the dissipation energy U_d are calculated by the following equations. Figure 13 represents the schematic diagram of uniaxial compression energy release in granite.

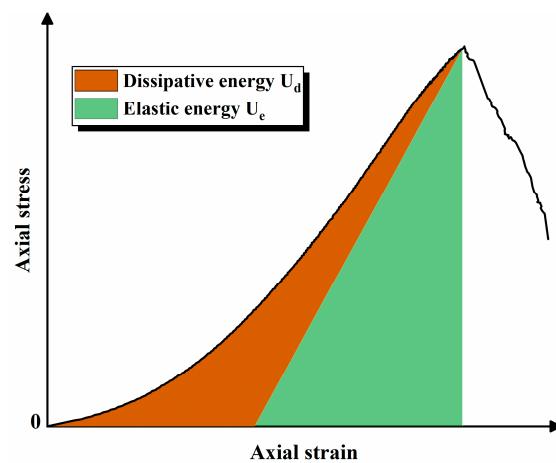


Figure 13. Schematic diagram of energy release.

$$U = U_e + U_d \quad (16)$$

$$U = \int \sigma_1 d\varepsilon_1 = \sum_{i=1}^n \frac{1}{2} (\sigma_1^i + \sigma_1^{i+1}) (\varepsilon_1^{i+1} - \varepsilon_1^i) \quad (17)$$

$$U_e = \frac{1}{2} \sigma_1 \varepsilon_1^e = \frac{\sigma_1^2}{2E} \quad (18)$$

$$U_d = U - U_e \quad (19)$$

where σ_1 and ε_1 represent axial stress and axial strain, respectively; E is the elastic modulus [47,48].

Figure 14 illustrates the relationship between total energy, elastic energy, dissipation energy and strain. As can be seen from the figure, in stage I (primary pore compaction stage), there are almost no significant changes in energy, producing small fluctuations. In stage II (linear elasticity stage), the deformation produced by granite in this process can be recovered, and the total energy appears to rise slightly, while the elastic energy and dissipation energy rise slowly, and the difference between the two energy values is very small. In stage III (crack stabilization and expansion stage), the total energy and elasticity energy rise faster than the dissipation energy, and there is a significant difference in the elastic energy and dissipated energy values, which are much larger than the dissipated energy. In stage IV (crack instability and expansion stage), the cracks begin to expand unsteadily, and the total energy and dissipation energy curves show a sudden change point, with a sharp increase, indicating the rapid release of granite energy. The cracks rapidly expand, penetrate, and gather to form macroscopic cracks. At the same time, mutation points can serve as precursors of rock instability. In stage V (destruction stage), when the stress reaches the peak intensity, the total energy, elastic energy and dissipation energy all reach the maximum value, and the dissipation energy shows a downward trend after the peak value, indicating the instability and failure of granite [49].

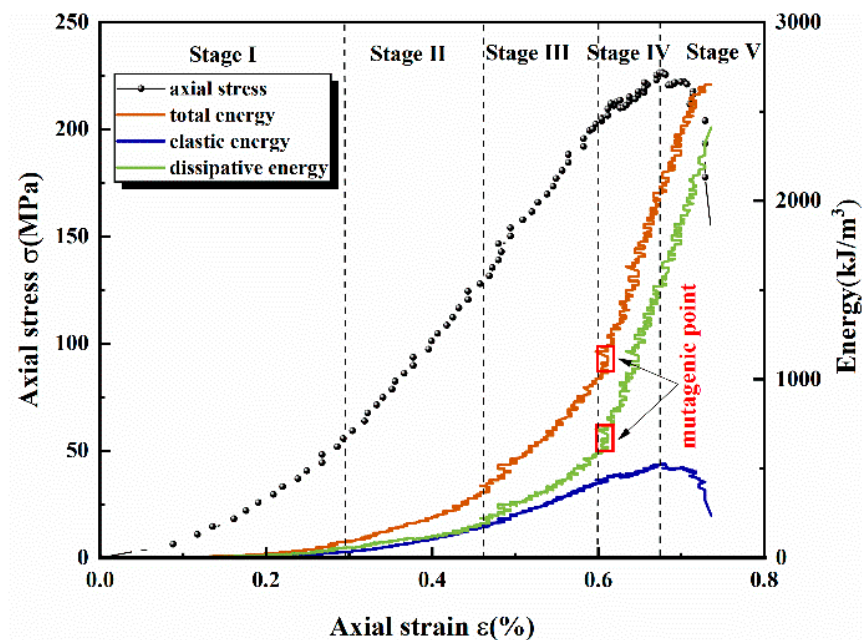


Figure 14. Relationship between energy and strain diagram.

In order to study the relationship between total energy, elastic energy, dissipation energy and strain under different powers, the energy evolution process of granite is further analyzed to reveal the damage process of granite under deep uniaxial compression. As shown in Figure 15. It can be seen from Figure 15a that as the cracks expand, the total energy

of the granite that has not been damaged by microwaves begins to increase significantly, and the difference from microwave-damaged granite is increasing. The difference in the total energy of the granite with 1 kW, 2 kW, and 3 kW is smaller. It is evident that during the pre-loading period, the primary pore compaction stage, and the linear elasticity stage, the microwave effect on the total energy is not obvious. As illustrated in Figure 15b, the overall trend of elastic energy variation with strain is very close to the trend of stress changes. During the pre-loading phase of granite, the discrepancy in elastic energy under different levels of power remains minimal. However, this difference becomes increasingly pronounced with the continual augmentation of axial force. The elastic strain energy reaches its peak value when the stress reaches its maximum intensity, and then rapidly decreases to a stable value. This phenomenon is primarily attributed to the friction between fracture surfaces, which prevents the elastic energy from diminishing to zero. The dissipation energy curve of granite (0 kW) in the initial loading phase aligns with the dissipated energy curve of microwave-damaged granite. In the crack expansion stage, the dissipation energy of granite (0 kW) escalates rapidly alongside the gradual increase in strain, with the disparity from others widening progressively. The dissipation energy for granite (1 kW, 2 kW, 3 kW) exhibits minor differences throughout the process, indicating a uniform behavior. It suggests that the dissipated energy in granite, at this juncture, is stored and subsequently released in various forms: plastic strain energy, kinetic energy resulting from damage, thermal energy due to friction, surface energy from crack propagation, and radiant energy from rupture, as referenced in studies [50,51].

$$\alpha = \frac{U_e}{U} \quad (20)$$

$$\beta = \frac{U_d}{U} \quad (21)$$

Figure 16 represents the amount and percentage of energy released by each part of granite under different powers. As can be seen from the figure, as the increase in microwave power, the total energy, elastic energy and dissipation energy decrease almost linearly. As the power increases from 0 kW to 3 kW, the total energy decreases from 948.9 kJ/m³ to 775.4 kJ/m³, a decrease of 22.4%; the elastic energy decreases from 522 kJ/m³ to 377.2 kJ/m³, a decrease of 38.4%; the dissipation energy decreases from 462.9 kJ/m³ to 398.2 kJ/m³, a decrease of 16.2%. It can be seen that the energy index further reflects that the microwave damage to granite is larger, and the microwave effect on the elastic energy is larger than the dissipation energy. The percentage of elastic energy α and dissipative energy β are calculated by the following formula, $\alpha + \beta = 1$ [52]. It can be seen from Figure 16 that the power increases from 0 kW to 2 kW, α decreases slowly while β rises slowly, and once the power rises to 3 kW, α decreases rapidly while β rises rapidly. The reason is that the higher the power, the greater the damage to the granite, and the more internal microcracks sprouted, resulting in the granite from elastic deformation tending to plastic deformation. The elastic energy is gradually converted to dissipative energy, resulting in a decrease in the proportion of elastic energy and a rise in the proportion of dissipative energy, and the phenomenon is more pronounced when the power is as high as a certain value [46].

Figure 17 shows the relationship between α and β and the strain of granite under different powers. As shown in Figure 17a, the changes in α and β of 0 kW granite are different from those of granite after microwave action, and the curves are similar to a "semicircle". From the primary pore compaction stage to the elastic deformation stage, α rises gradually with the increase in strain and the rate of increase slows down, while β behaves in the opposite way, and α and β are equal with the value of 50% at a strain of about 0.45%. It can be considered that this particular point is a sign of the beginning of the stable crack expansion stage, and the change in α and β is slower. When the crack begins to expand unstably, α and β change very rapidly, and there is no change until the stress reaches the peak value. The reason is that the granite without microwave damage

has stronger strength and deformation capacity, and stores more elastic energy. So, the elastic energy is converted into more dissipative energy in the later loading, which shows a decrease in the latter part of the α curve. From Figure 17b–d, it can be seen that the overall changes in α and β in the granite subjected to microwave damage are similar. With α increasing gradually from the beginning to the maximum when the stress reaches the peak, and α decreases and β rises instead after the peak. This is mainly due to the fact that granite maintains a certain post-peak residual strength after destruction, and part of the elastic energy is stored in the granite and not released. It is worth noting that α and β of granite with a power of 1 kW are equal at the point of strain of about 0.58% and are in the stage of unstable expansion of cracks; α and β of granite with a power of 2 kW are equal at the point of strain about 0.6% and are in the stage of unstable expansion of cracks. α and β of granite with a power of 3 kW are equal at the point of strain about 0.68% and are just at the peak point. It can be seen that the point of equality between the elastic and dissipative energy ratios is delayed with the higher power. The author believes that under microwave damage, the dominant position of elastic energy is becoming lower and lower, which is not enough to show that the elastic energy ratio exceeds the dissipative energy ratio in the later loading, thus leading to the intersection point of α and β curves being gradually shifted back, or even no intersection point. Even there is no intersection point, which further indicates that the greater the degree of microwave damage, the weaker the capacity of the elastic energy stored in the granite, and the proportion of elastic energy released decreases [53]. Based on the energy dissipation theory exploring the energy evolution characteristics of granite under different powers, consistent with the results of previous studies, this study has practical value and provides a method for the study of microwave-assisted rock breaking.

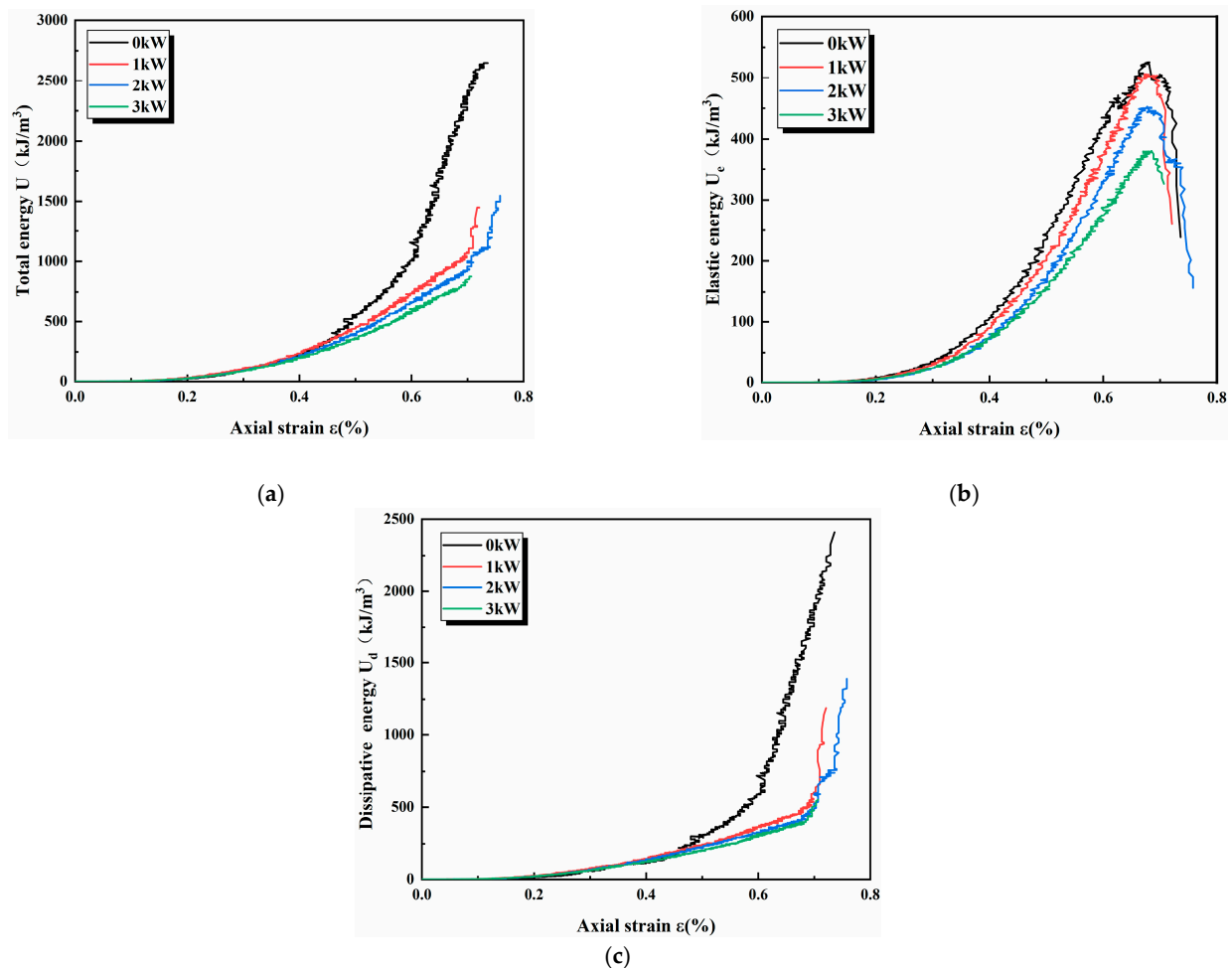


Figure 15. Relationship between the energy of each component and strain. (a) U ; (b) U_e ; (c) U_d .

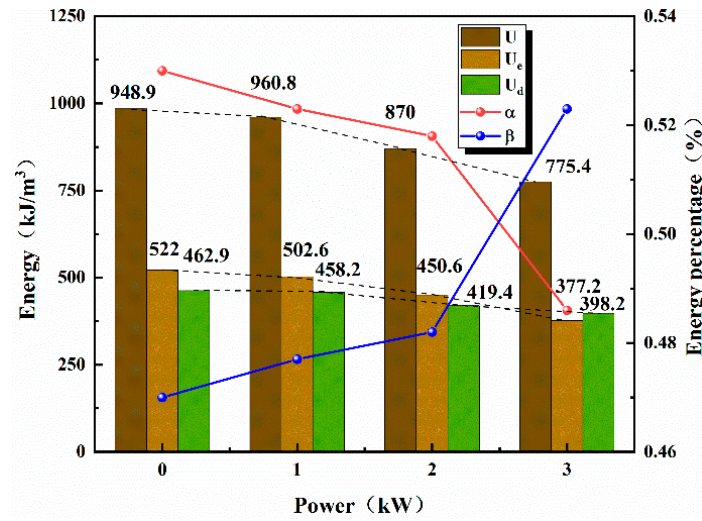


Figure 16. Relationship between energy and microwave power.

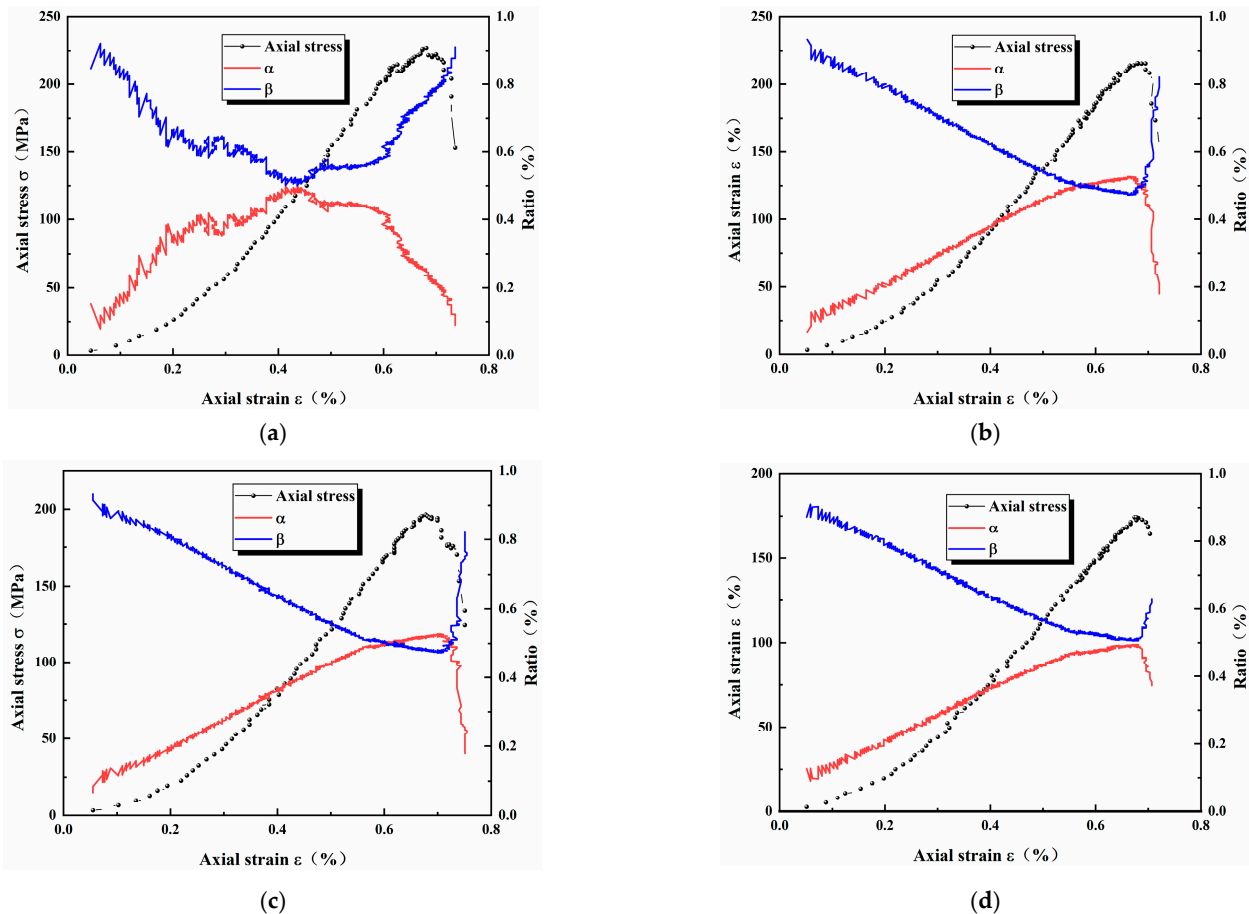


Figure 17. Relationship between energy ratio and strain. (a) P = 0 kW; (b) P = 1 kW; (c) P = 2 kW; (d) P = 3 kW.

6. Conclusions

In order to study the dynamic response of granite under different microwave powers, the following conclusions were drawn based on NMR (nuclear magnetic resonance) analysis of the degree of pore damage, and also based on the energy dissipation energy theory to analyze the energy evolution process of granite under different powers.

(1) Microwave pore damage is very obvious to granite; the higher the power, the greater the porosity, and the micropores are more sensitive to microwaves. The higher the power, the lower the peak strength and elastic modulus of granite, and the more obvious the degree of fragmentation, showing the characteristics of large damage at the two ends and small damage in the middle.

(2) Granite gradually changes from elastic to plastic deformation, the ratio of elastic energy decreases and the ratio of dissipation energy increases, and the greater the power, the more serious the damage. Furthermore, the higher the power, the lower the total energy, elastic energy, and dissipation energy.

(3) Studying the pore changes and energy evolution of granite under different powers of microwave can better control the microwave power in real engineering, improve economic efficiency, reduce the waste of resources, and reduce the TBM (tunnel boring machine) blade wear problem.

Author Contributions: Writing—original draft preparation, Y.Z.; Validation, K.Z.; Supervision, Z.P. and C.Y.; Writing—review and editing, all authors. All authors have read and agreed to the published version of the manuscript.

Funding: This study was financially supported by the Fundamental Research Funds for the Central Universities of Central South University (2023ZZTS0498, 2023ZZTS0715), the National Natural Science Foundation of China (Project no. 52204167), and the Open Research Fund of State Key Laboratory of Safety Technology of Metal Mines (Project no. kfkt2023-04).

Institutional Review Board Statement: Not applicable.

Data Availability Statement: The source data can be obtained in the article.

Conflicts of Interest: The authors declare no conflicts of interest.

References

1. Wang, J.C.; Jiang, F.X.; Meng, X.J.; Wang, X.Y.; Zhu, S.T.; Feng, Y. Mechanism of Rock Burst Occurrence in Specially Thick Coal Seam with Rock Parting. *Rock Mech. Rock Eng.* **2016**, *49*, 1953–1965. [[CrossRef](#)]
2. Lu, G.M.; Li, Y.H.; Hassani, F.; Zhang, X.W. Review of theoretical and experimental studies on mechanical rock fragmentation using microwave-assisted approach. *Chin. J. Geotech. Eng.* **2016**, *38*, 1497–1506.
3. Yang, C.; Hassani, F.; Zhou, K.P.; Zhang, Q.; Wang, F.M.; Gao, F.; Topa, A. Numerical investigation of TBM disc cutter cutting on microwave-treated basalt with an unrelieved model. *Arch. Civ. Mech. Eng.* **2020**, *22*, 147. [[CrossRef](#)]
4. Yang, C.; Hassani, F.; Zhou, K.P.; Xiong, X.; Wang, F.M.; Shao, Y. Effect of microwave treatment on the thermal properties and dynamic splitting behavior of red sandstone. *Can. Geotech. J.* **2022**, *59*, 1231–1242. [[CrossRef](#)]
5. Yang, C.; Hassani, F.; Zhou, K.P.; Gao, F.; Topa, A. SPH-FEM simulations of microwave-treated basalt strength. *Trans. Nonferrous Met. Soc. China.* **2022**, *32*, 2003–2018. [[CrossRef](#)]
6. Ma, Z.J.; Zheng, Y.L.; Zhao, X.B.; Li, J.C. Microwave-assisted hard rock breakage by impact hammers: Heating, fracturing and mechanical breakage. *Bull. Assoc. Int. Geol. Ing. Environ.* **2022**, *81*, 308. [[CrossRef](#)]
7. Feng, X.T.; Li, S.P.; Yang, C.X.; Lin, F.; Tong, T.Y.; Su, X.X.; Zhang, J.Y. The Influence of the Rotary Speed of a Microwave Applicator on Hard-Rock Fracturing Effect. *Rock Mech. Rock Eng.* **2022**, *55*, 6963–6979. [[CrossRef](#)]
8. Zou, C.J.; Quan, X.; Ma, Z.J.; Zheng, Y.L.; Zhao, X.B.; Li, J.C.; Zhao, J. Dynamic Strength and Indentation Hardness of a Hard Rock Treated by Microwave and the Influence on Excavation Rate. *Rock Mech. Rock Eng.* **2023**, *56*, 4535–4555. [[CrossRef](#)]
9. Zhao, Q.H.; Zhao, X.B.; Zheng, Y.L.; Li, J.C.; He, L.; Zou, C.J. Microwave fracturing of water-bearing sandstones: Heating characteristics and bursting. *Int. J. Rock Mech. Min. Sci.* **2021**, *136*, 104495. [[CrossRef](#)]
10. Zhao, Q.H.; Zhao, X.B.; Zheng, Y.L.; Li, J.C.; He, L.; Zou, C.J. Heating characteristics of igneous rock-forming minerals under microwave irradiation. *Int. J. Rock Mech. Min. Sci.* **2020**, *135*, 104519. [[CrossRef](#)]
11. Gao, F.; He, Y.D.; Xiong, X.; Zhou, K.P.; Yang, C. Effect of strong dielectric substances on the damage characteristics of rocks exposed to microwave radiation: Insight from experiments and mechanisms. *Int. J. Damage Mech.* **2023**, *32*, 849–871. [[CrossRef](#)]
12. Cheng, S.T. *Study on the Influence of Heating Method on Thermal Induced Damage of Granite*; Beijing University of Technology: Beijing, China, 2020.
13. Gao, F.; Shao, Y.; Xiong, X.; Zhou, K.P.; Cao, S.P. Rising characteristics of internal and external temperatures of rock specimens under different microwave irradiation modes. *Chin. J. Geotech. Eng.* **2020**, *42*, 650–657.
14. Xu, S.L. *Experimental Research on Damage Characteristics of Basalt by Microwave Cyclic Irradiation*; Xi'an University of Science and Technology: Xi'an, China, 2019.
15. Yang, J.M.; Liu, J.T.; Guo, H.C.; Li, Q.M.; Wang, W. Effect of microwave heating on the mechanical properties and energy dissipation characteristics of hard rock. *Environ. Earth Sci.* **2022**, *81*, 415. [[CrossRef](#)]

16. Tang, M.Y.; Gao, M.Z.; Li, S.W.; Yang, B.G.; Tang, R.F.; Li, F.; Liu, J.J. Failure behavior and energy evolution characteristics of deep roadway sandstone under different microwave irradiation modes. *J. Cent. South Univ.* **2023**, *30*, 214–226. [[CrossRef](#)]
17. Hassani, F.; Shadi, A.; Rafezi, H.; Sasmito, A.P.; Ghoreishi-Madiseh, S.A. Energy analysis of the effectiveness of microwave-assisted fragmentation. *Miner. Eng.* **2020**, *159*, 106642. [[CrossRef](#)]
18. Pressacco, M.; Kangas, J.J.; Saksala, T. Numerical Modelling of Microwave Heating Assisted Rock Fracture. *Rock Mech. Rock Eng.* **2022**, *55*, 481–503. [[CrossRef](#)]
19. Pressacco, M.; Kangas, J.J.; Saksala, T. Numerical modelling of microwave irradiated rock fracture. *Miner. Eng.* **2023**, *203*, 108318. [[CrossRef](#)]
20. Zhao, X.B.; Zhao, Q.H.; Zheng, Y.L.; He, L.; He, J.L.; Zhao, G.F.; Li, H. Cracking Behavior and Mechanism of Igneous Rocks Under Open-Ended Microwave Irradiation. *Rock Mech. Rock Eng.* **2022**, *55*, 6151–6169. [[CrossRef](#)]
21. Rui, F.X.; Zhao, G.F.; Zhang, Y.L.; Fan, L.F.; Zhao, X.B. Study on the Mechanism of Rock Damage Under Microwave and Laser Irradiation Through Multiscale and Multiphysics Numerical Modelling. *Rock Mech. Rock Eng.* **2023**, *57*, 1079–1102. [[CrossRef](#)]
22. Lu, G.M.; Li, Y.H.; Hassani, F.; Zhang, X.W. The influence of microwave irradiation on thermal properties of main rock-forming minerals. *Appl. Therm. Eng.* **2017**, *112*, 1523–1532. [[CrossRef](#)]
23. Tian, J.; Lu, G.M.; Feng, X.T.; Li, Y.H.; Zhang, X.W. Experimental study of the microwave sensitivity of main rock-forming mineral. *Rock Soil Mech.* **2019**, *40*, 2066–2074.
24. Hartlieb, P.; Toifl, M.; Kuchar, F.; Meisels, R.; Antretter, T. Thermo-physical properties of selected hard rocks and their relation to microwave-assisted comminution. *Miner. Eng.* **2016**, *91*, 34–41. [[CrossRef](#)]
25. Lu, G.M.; Feng, X.T.; Li, Y.H.; Hassani, F.; Zhang, X.W. Experimental Investigation on the Effects of Microwave Treatment on Basalt Heating, Mechanical Strength, and Fragmentation. *Rock Mech. Rock Eng.* **2019**, *52*, 2535–2549. [[CrossRef](#)]
26. Wang, H.C.; Rezaee, R.; Saeedi, A. Preliminary study of improving reservoir quality of tight gas sands in the near wellbore region by microwave heating. *J. Nat. Gas Sci. Eng.* **2016**, *32*, 395–406. [[CrossRef](#)]
27. Bilali, L.; Benchanaa, A.; El, H.K.; Mokhlisse, A.; Outzourhit, A. A detailed study of the microwave pyrolysis of the Moroccan (Youssoufia) rock phosphate. *J. Anal. Appl. Pyrolysis* **2005**, *73*, 1–15. [[CrossRef](#)]
28. Yao, J.H.; Tao, M.; Zhao, R.; Hashemi, S.S.; Wang, Y.Q. Effect of microwave treatment on thermal properties and structural degradation of red sandstone in rock excavation. *Miner. Eng.* **2021**, *162*, 106730. [[CrossRef](#)]
29. Li, X.B.; Wu, Y.C.; Li, Q.; Yin, T.B.; Huang, L.Q. Quantification of thermal damage and dynamic tensile behaviors of hard rock under microwave irradiation: An experimental investigation. *Bull. Eng. Geol. Environ.* **2022**, *81*, 461. [[CrossRef](#)]
30. Ding, R.; Sun, Q.; Geng, J.S.; Luo, T.; Yuan, S.H. Porosity and mechanical strength of microwave-heated gabbro. *Geomech. Geophys. Geo-Energy Geo-Resour.* **2022**, *8*, 196. [[CrossRef](#)]
31. Li, J.L.; Zhu, L.Y.; Zhou, K.P.; Liu, H.W.; Cao, S.P. Damage characteristics of sandstone pore structure under freeze-cycles. *Rock Soil Mech.* **2019**, *40*, 3524–3532.
32. Pan, Z.; Zhou, K.P.; Gao, R.G.; Jiang, Z.; Yang, C.; Gao, F. Research on the Pore Evolution of Sandstone in Cold Regions under Freeze-Thaw Weathering Cycles Based on NMR. *Geofluids* **2020**, *2020*, 884944. [[CrossRef](#)]
33. Yan, J.P.; Wen, D.N.; Li, Z.Z.; Geng, B.; Cai, J.G.; Ling, Q.; Yun, Y. The Quantitative evaluation method of low permeable sandstone pore structure based on nuclear magnetic resonance(NMR) logging. *Chin. J. Geophys.* **2016**, *59*, 1543–1552.
34. Jiang, Z.; He, H.; Tian, G.L.; Guo, W.Z.; Li, Y.Z.; Pan, Z. Pore Structure Quantification and Fractal Characterization of MSA Mortar Based on 1H Low-Field NMR. *Fractal Fract.* **2024**, *8*, 42. [[CrossRef](#)]
35. Pan, Z.; Zhou, K.; Wang, Y.; Lin, Y.; Saleem, F. Comparative Analysis of Strength and Deformation Behavior of Cemented Tailings Backfill under Curing Temperature Effect. *Materials* **2022**, *15*, 3491. [[CrossRef](#)]
36. Rui, F.X.; Zhao, G.F. Experimental and numerical investigation of laserinduced rock damage and the implications for laser-assisted rock cutting. *Int. J. Rock. Mech. Min. Sci.* **2021**, *139*, 104653. [[CrossRef](#)]
37. Hu, G.Z.; Zhu, J.Q.; Sun, C.; Yang, N.; Qin, W. Fracturing effect and damage behaviors for microstructure in shale under microwave irradiation. *J. China Coal Soc.* **2020**, *45*, 3471–3479.
38. Zhang, W.Q. *Study on the Microscopic Mechanism of Rock Thermal Damage and the Evolution Characteristics of Macroscopic Physical and Mechanical Properties*; China University of Mining and Technology: Xuzhou, China, 2017.
39. Gao, M.Z.; Xie, J.; Yang, B.G.; Tang, R.F.; Deng, H.C.; Liu, Y.T.; Ye, S.Q.; Zhou, X.M.; Wang, S.L. Characteristics and mechanism of rock 3D volume fracturing in microwave field. *J. China Coal Soc.* **2022**, *47*, 1122–1137.
40. Li, J.L.; Kaunda, R.B.; Rrora, S.; Hartlieb, P.; Nelson, P.P. Fully-coupled simulations of thermally-induced cracking in pegmatite due to microwave irradiation. *J. Rock Mech. Geotech. Eng.* **2019**, *11*, 242–250. [[CrossRef](#)]
41. Liu, G.M.; Feng, X.T.; Li, Y.H.; Zhang, X.W. Influence of microwave treatment on mechanical behaviour of compact basalts under different confining pressures. *J. Rock Mech. Geotech. Eng.* **2020**, *12*, 213–222. [[CrossRef](#)]
42. Zhang, C.Y.; Liu, T.Y.; Jiang, C.; Zhao, C.; Chen, Z.; Zhou, K.P.; Chen, L.J. The Freeze-Thaw Strength Evolution of Fiber-Reinforced Cement Mortar Based on NMR and Fractal Theory: Considering Porosity and Pore Distribution. *Materials* **2022**, *15*, 7316. [[CrossRef](#)]
43. Porteneuve, C.; Korb, J.P.; Petit, D.; Zanni, H. Structure–texture correlation in ultra-high-performance concrete: A nuclear magnetic resonance study. *Cem. Concr. Res.* **2002**, *32*, 97–101. [[CrossRef](#)]
44. Gao, F.; Xiong, X.; Zhou, K.P.; Li, J.L.; Shi, W.C. Strength deterioration model of saturated sandstone under freeze-thaw cycles. *Rock Soil Mech.* **2019**, *40*, 926–932.

45. Gao, F.; Cao, S.P.; Zhou, K.P.; Lin, Y.; Zhu, L.Y. Damage characteristics and energy-dissipation mechanism of frozen–thawed sandstone subjected to loading. *Cold Reg. Sci. Technol.* **2020**, *169*, 102920. [[CrossRef](#)]
46. Gong, F.Q.; Zhang, P.L.; Xu, L. Damage constitutive model of brittle rock under uniaxial compression based on linear energy dissipation law. *Int. J. Rock Mech. Min. Sci.* **2022**, *160*, 105273. [[CrossRef](#)]
47. Gong, F.Q.; Zhang, P.L.; Luo, S.; Li, J.C.; Huang, D. Theoretical damage characterisation and damage evolution process of intact rocks based on linear energy dissipation law under uniaxial compression. *Int. J. Rock Mech. Min. Sci.* **2021**, *146*, 104858. [[CrossRef](#)]
48. Yan, J.Y.; Gong, F.Q.; Luo, S. Effects of length-to-diameter ratio on energy storage characteristics of rock materials under uniaxial compression. *Bull. Eng. Geol. Environ.* **2022**, *81*, 508. [[CrossRef](#)]
49. Wang, Z.L.; Li, S.Y.; Wang, J.G.; Xiong, F.; Xie, L.X. Mechanical behavior, mesoscopic properties and energy evolution of deeply buried marble during triaxial loading. *Int. J. Damage Mech.* **2022**, *31*, 1592–1612. [[CrossRef](#)]
50. Dong, Y.X. *Study on Rock Deformation and Strength Characteristics under Loading and Unloading after High Temperature*; China University of Mining and Technology: Xuzhou, China, 2020.
51. Luo, Y.; Gong, H.L.; Xu, K.; Pei, C.H.; Wei, X.Q.; Li, X.P. Progressive failure characteristic and energy accumulation of granite with a pre-fabricated fracture during conventional triaxial loading. *Theor. Appl. Fract. Mech.* **2022**, *118*, 103219. [[CrossRef](#)]
52. Li, C.; Mo, P.Q.; Li, S.C. Stability analysis of energy dissipation mechanisms in rocks surrounding circular opening. *Appl. Math. Model.* **2024**, *127*, 327–342. [[CrossRef](#)]
53. Zhu, X.H.; Liu, W.J. The rock fragmentation mechanism and plastic energy dissipation analysis of rock indentation. *Geomech. Eng.* **2018**, *16*, 195–204.

Disclaimer/Publisher’s Note: The statements, opinions and data contained in all publications are solely those of the individual author(s) and contributor(s) and not of MDPI and/or the editor(s). MDPI and/or the editor(s) disclaim responsibility for any injury to people or property resulting from any ideas, methods, instructions or products referred to in the content.